Enhanced sparse component analysis for operational modal identification of real-life bridge structures

Yan Xu[a], James Brownjohn[a], David Hester[b]

[a]Vibration Engineering Section, College of Engineering, Mathematics and Physical Sciences, University of Exeter, UK

[b]School of Natural and Built Environment, Queen's University Belfast, UK

Abstract:

Blind source separation receives increasing attention as an alternative tool for operational modal analysis in civil applications. However, the implementations on real-life structures in literature are rare, especially in the case of using limited sensors. In this study, an enhanced version of sparse component analysis is proposed for output-only modal identification with less user involvement compared with the existing work. The method is validated on ambient and non-stationary vibration signals collected from two bridge structures with the working performance evaluated by the classic operational modal analysis methods, stochastic subspace identification and natural excitation technique combined with the eigensystem realisation algorithm (NExT/ERA). Analysis results indicate that the method is capable of providing comparative results about modal parameters as the NExT/ERA for ambient vibration data. The method is also effective in analysing non-stationary signals due to heavy truck loads or human excitations and capturing small changes in mode shapes and modal frequencies of bridges. Additionally, closely-spaced and low-energy modes can be easily identified. The proposed method indicates the potential for automatic modal identification on field test data.

Keywords: Blind source separation; sparse component analysis; operational modal identification; non-stationary signals.

1 INTRODUCTION

Operational modal analysis (OMA) is targeted at identifying modal characteristics from only response measurements of structures under ambient or natural excitation [1] and has many applications such as for structural identification, vibration-based health monitoring and damage detection, etc.

Several algorithms have been developed for OMA, including natural excitation technique combined with the eigensystem realisation algorithm (NExT/ERA) [2,3], stochastic subspace identification (SSI) approaches [4] and a general auto-regression moving average (ARMA) model [5] in time domain and frequency domain decomposition [6] in frequency domain. Most of them are parametric identification methods based on a mathematical model representing the physical phenomenon of structural dynamics. Their applications are limited to certain situations (e.g. ambient and free vibration signals) due to the model assumption regarding the nature of excitation forces (e.g. a broadband uncorrelated random process). In addition, the working performance is sensitive to some model parameters (e.g. model order) and the parameter selection is dependent on users' subjective judgement.

Hilbert Huang transform (HHT) [7–9] is a parameter-free time-frequency analysis tool for modal identification which is capable of dealing with nonlinear and nonstationary signals. One critical step in the HHT is empirical mode decomposition (EMD), i.e. decomposing one multi-component signal into a series of mono-component signals. The decomposition process exploits no joint information between multiple measurement channels and might derive modal responses involving mode mixing [10]. Improved work has been performed by proposing the ensemble EMD [11] and multivariate EMD [12,13] to overcome limitations.

Blind source separation (BSS) offers an alternative for OMA, belonging to non-parametric identification methods. BSS originates from the audio signal processing field for de-mixing audio sources from recordings via a mixing matrix. Its physical interpretation for OMA is that with the modal responses regarded as virtual sources, the mixing matrix is mapped directly to structural vibration modes [14]. BSS is classified into two types, overdetermined and undetermined cases depending on the provided measurement channels compared to the number of active modes. Underdetermined BSS is suitable for civil applications with limited sensors available and has been addressed by different methods such as sparse component analysis (SCA) and tensor decomposition.

The SCA makes use of sparseness in the transformed domain i.e. the time-frequency (TF) domain for decomposition. The sources are assumed to be sparsely represented after the TF transform e.g. short-time Fourier transform (STFT) [15] [16] [17], wavelet packet transform [18] and quadratic TF transform [19]. A mixing matrix (or mode shapes) is estimated using clustering algorithms (e.g. hierarchical clustering [15], K-hyperline clustering [16], K-means clustering [17] [19] and Fuzzy C-means clustering [20]) on scatter plots of measurement signals in the transformed domain. Given the mixing matrix, source signals can be reconstructed based on the source sparsity using l^1 norm minimisation [16] [20], smoothed zero-norm algorithm [15] or subspace-based algorithm (by identifying active sources at TF points and estimating the energy each of these sources contributes) [19]. With the source signals (or modal responses) available, modal frequencies and damping ratios can be estimated using either single-mode curve fitting in frequency domain or logarithmic decrement method in time domain. The SCA has been implemented for OMA on a cantilever beam structure [16], a laboratory tower structure under narrow-band excitations [18] and a column structure in temperature-varying environment [17] with the working performance evaluated against identification using SSI [16].

Tensor decomposition method is an alternative for the underdetermined BSS based on the assumption that source signals are uncorrelated among different channels but correlated individually in time [21]. The main idea is to decompose the third-order tensor representation (i.e. spatial covariance matrices of observation signals for different time lags) into a linear combination of a minimal number of rank-1 terms by means of an alternating least squares algorithm. The derived mixing matrix and autocovariance of modal responses can be used for modal parameter estimation. The method has been validated at being effective when analysing ambient vibration signals [22], earthquake responses [23] as well as human-induced vibrations [24] [25].

Although there are already a few studies implementing the underdetermined BSS for OMA, most of these are numerical and laboratory studies, while field tests are rare except on two footbridges [25,26], one tower structure [27] and two buildings [28,29]. There is no further study to investigate whether the underdetermined BSS method is capable of offering an effective alternative to classic OMA methods on field testing data, especially non-stationary vibration signals.

In this study, an enhanced method based on the SCA is proposed for OMA suitable for field applications. In this method, a novel procedure of the two-step clustering is involved to ensure an automatic and robust estimation of mode shapes that is the basis for the accurate estimation of modal parameters. The proposed method is validated on two full-scale in-operation bridges in both ambient and non-stationary vibrations (i.e. due to heavy truck loads or passing pedestrians). Wired and wireless accelerometer sensors with different accuracy levels were used for data acquisition to test the sensitivity of the proposed method to noise level. Closely-spaced and low-energy modes that are common for footbridges are considered based on the recorded data. The working performance of the proposed method is evaluated by comparing with the classic OMA methods i.e. NExT/ERA and SSI.

To that end, section 2 introduces the main methodologies of the proposed OMA method based on the SCA and improvements, mainly in the clustering step, to ensure a robust estimation of mode shapes. Section 3 describes a validation study on ambient vibrations of a short-span road bridge and evaluates the performance through comparing the results with those using the NExT/ERA algorithm. Section 4 describes a load test on the same bridge and investigates the feasibility of the proposed method on non-stationary signals. Section 5 analyses non-stationary vibration data from a footbridge under pedestrian excitation and validates the effectiveness of the proposed method for vibration signals under narrow-band excitation and for extracting closely-spaced modes.

2 ENHANCED SPARSE COMPONENT ANALYSIS FOR OMA

The BSS is a powerful tool for separating mixed signals when the sources and the mixing methodology are unknown. The simple form of BSS in the noiseless case is to determine a mixing matrix A (using statistical and data structure information [30]) and to recover the M-component source data $\mathbf{s}$ from their linear mixture in the N-component observational data $\mathbf{X}$, expressed as

$$\mathbf{X}(t) = \mathrm{A}\,\mathbf{s}(t)\,. \tag{1}$$

Consistent with the expression in BSS, the vibration measurement $\mathbf{X}$ could be decomposed via the mode shape matrix $\mathbf{\Phi}$ A into single-mode response signals $q(t)$, similar to the BSS expression in Equation (1).

$$\mathbf{X}(t) = \mathbf{\Phi} q(t)\,. \tag{2}$$

Thus, BSS methods have been successfully utilised for OMA [30], i.e. estimating mode shapes and identifying modal parameters from the recovered single-mode response signals $q(t)$.

The case of underdetermined BSS, where the number of active modes is larger than the number of measurement channels (M>N), is common for civil applications. To solve the underdetermined BSS problem, the SCA provides a simple framework based on source sparseness [31]. The main algorithms and procedures of the SCA are presented in section 2.1; and an enhanced SCA targeted for OMA in civil applications is described in section 2.2.

2.1 Sparse component analysis for OMA

SCA is a relatively simple tool for separating a number of sources from observed mixtures, primarily for underdetermined cases. The underlying assumption is data sparsity, e.g. at each point t, a single source is significantly more active than others [31]. In a scatter plot of observational data mixtures, the collection of points dominated by the same source signal forms into one straight line passing the origin and could be separated as one cluster with the line direction representing the mixing vector.

The original form of data mixture generally does not fit the assumption about sparsity. Figure 1(a) demonstrates the temporal scatter plot of two mixture signals ($x_1(t)$ and $x_2(t)$) from five sources (data from the numerical example in section 2.3). The figure indicate no apparent line alignment and the sources could not be regarded as disjoint support in time domain. Therefore, a pre-processing step i.e. sparse signal representation is essential before any clustering.

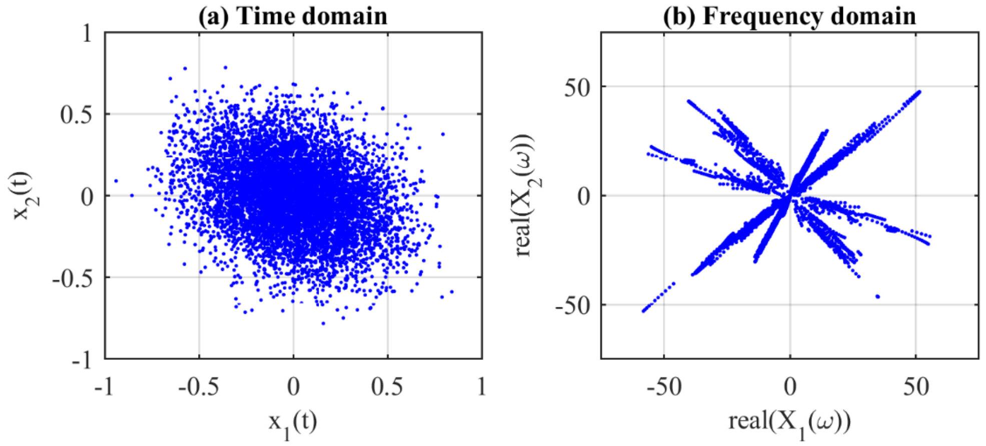

Figure 1 Scatter plots of two-channel signals (involving five sources) in time domain (a) and frequency domain (b).

A sparse representation of observed mixtures could facilitate the mixing matrix estimation. Linear time-frequency (TF) transforms like short-time Fourier transform (STFT) and wavelet transform are commonly applied to measured signals of each channel ($c_{\mathbf{X}}^{\Psi} := \mathbf{X}\Psi$) for sparsity. Through the linearity of the transform, the source separation problem has an exact analogue in the transformed domain as

$$C_{\mathbf{X}}^{\Psi}(k) = \mathrm{A}C_{\mathrm{s}}^{\Psi}(k) \tag{3}$$

and the sources $C_s^{\Psi}(k)$ in the transformed domain are expected to be reasonably disjoint. Figure 1 (b) presents the TF scatter plot of the two-channel signals, indicating approximately directions of five aligned straight lines.

The second step of SCA consists of estimating the mixing matrix by means of clustering from a scatter plot of the TF coefficients $\{C_X^{\Psi}(k)\}$. The performance of mixing matrix estimation using a clustering algorithm degrades when the sources are non-disjoint in the transformed domain. This problem could be resolved by refining the TF coefficients $\{C_X^{\Psi}(k)\}$ for clustering through detecting only single source points (SSPs) i.e. where a single source dominates. The common criteria for SSP detection include the complex ratio of the mixtures over a small window in the transformed domain [17,32] and directional alignment of the real and imaginary parts of TF coefficients [33][15]. Scatter plots of sparse coefficients $\{C_X^{\Psi}(k_i)\}$ yield clear lines of orientation corresponding to the vectors constituting the mixing matrix. For convenience, unit vectors of the normalised TF coefficients $\{\bar{C}_X^{\Psi}(k_i)\}$ are imported for classification with cluster centroids denoting the mixing matrix or mode shapes directly. Clustering algorithms used for OMA applications include hierarchical clustering algorithm [33][15], K-means algorithm [17][19], K-hyperline clustering [16] and Fuzzy C-Means clustering [20].

Given the estimated mixing matrix $\hat{A}$, the source TF representation $C_s^{\Psi}(k)$ in Equation (3) is estimated based on the source sparsity by finding the solution that minimises the l^q norm [34],

$$\hat{C}_s^{\Psi}(k) := \arg\min \left\| C_s^{\Psi} \right\|_q \text{ subject to } \hat{A} C_s^{\Psi}(k) = C_X^{\Psi}(k), \qquad q \le 1. \tag{4}$$

For example, l^1 norm minimisation could be interpreted as a maximum likelihood estimate of source TF coefficients assuming the coefficients have a Laplacian distribution. The sparsity criteria used in literature include l^1 norm [16,20] and an improved l^0 norm named smoothed zero norm algorithm [15].

In the fourth step, source signals are reconstructed to the time domain by inverse TF transform. Finally, the modal parameters can be extracted from source signals (modal responses) by using either single-mode curve fitting in frequency domain or logarithmic decrement method in time domain. The SCA flowchart is summarised in Figure 2; further details can be found in [17][31].

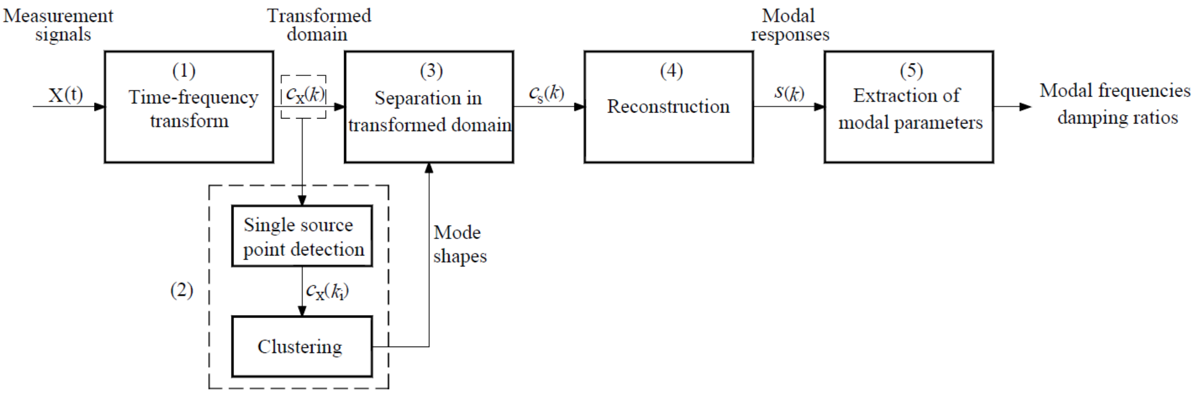

Figure 2 Flowchart of the SCA for OMA (modified from Figure 10.2 in [31]).

2.2 *Enhanced sparse component analysis*

Accurate estimates of mode shapes in the second step are critical for the robustness of source separation that has direct influence on the accuracy of identified modal parameters. The existing problem in the SCA method for OMA is that some mode shapes of a structural system estimated based on limited sensors are of high similarity and might be incorrectly assigned to one cluster, contributing together for the estimation of a single mode shape. For example, torsion modes could not be distinguished from bending modes by the SCA method when sensors for data collection are located on one longitudinal side of a bridge structure.

Compared with existing work [15–20] implementing the SCA method for OMA, the proposed method in this study made improvement to the second step, mode shape estimation. To overcome the ambiguity of mode shape representation using limited sensors, a novel two-step clustering procedure is shown in Figure 3, i.e. first clustering frequency values $\{f(k)\}$ and then clustering TF coefficients $\{C_{\mathrm{X}}^{\Psi}(k)\}$. After TF transform of measurement signals in the first step, both the TF coefficients $\{C_{\mathrm{X}}^{\Psi}(k)\}$ and the corresponding frequency values $\{f(k)\}$ are stored for analysis. The SSPs are detected using a threshold angle $\Delta\theta$ based on directional alignment of the real parts ($R\{C_{\mathrm{X}}^{\Psi}(k)\}$) and the imaginary parts ($I\{C_{\mathrm{X}}^{\Psi}(k)\}$) in TF coefficients [33] expressed as

$$\left| \frac{R\{C_{\mathrm{X}}^{\Psi}(k)\}^{T} I\{C_{\mathrm{X}}^{\Psi}(k)\}}{\left\| R\{C_{\mathrm{X}}^{\Psi}(k)\} \right\| \cdot \left\| I\{C_{\mathrm{X}}^{\Psi}(k)\} \right\|} \right| > \cos(\Delta\theta) . \tag{5}$$

Instead of clustering TF coefficients directly for mode shape estimation, a frequency-clustering step is added to avoid any ambiguity of mode shape representation. The stored frequency values of these identified SSPs are analysed first using hierarchical clustering, leading to a few groups of SSPs with different frequency ranges. Since similar modes based on limited sensors usually have apparent deviations in modal frequency values, the purpose of this step is to separate them into different groups before clustering TF coefficients. Note that this step is not aimed at modal frequency estimation and also it is acceptable to include several closely-spaced modes into one group.

For each group of SSPs, the normalised TF coefficients are clustered to identify mode shape candidates which are real-valued. Implementation of some clustering methods used in literature like K-means and Fuzzy C-Means requires prior specification of the number of clusters. This is problematic as the existing mode number in measurement signals is unknown before the analysis. Another problem in these methods is the sensitivity to the initialisation and that poor choices of initialised cluster centroids can lead to sub-optimal configuration of cluster assignment.

In this study, a probabilistic method using Dirichlet process mixture models [35] is used for cluster analysis of the TF coefficients. The main idea of this method is to fit the data to a Dirichlet process mixture model (i.e. an infinite mixture model) that maximises the overall posterior probability of cluster assignment. As a random variable in the model, the number of clusters is estimated as an intrinsic part of the algorithm. This clustering method has been validated to be robust to the presence of outliers (by assigning them into separate clusters) [35] that is common for data collected from field tests. Detailed description of this method is in the reference [35].

Among the extracted mode shape candidates, outliers are automatically removed according to a minimum sample number and statistical information about sample distribution in each cluster using two parameters, standard deviations of modal frequency values and standard deviations of point distance to the cluster centroid.

Procedures (steps 3-5) after mode shape estimation follow the SCA flowchart in Figure 2.

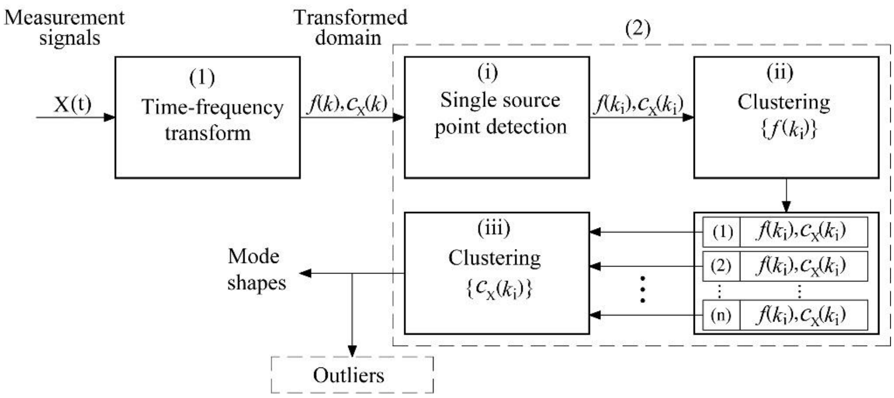

Figure 3 Procedures of mode shape estimation using two-step clustering proposed in this study

2.3 Numerical illustration

A five degree-of-freedom (DOF) building model [25] is set up to validate the proposed method. The natural frequencies are 0.91 Hz, 3.37 Hz, 7.11 Hz, 10.66 Hz and 12.73 Hz while damping ratios are assumed as 2% in all modes. The system is excited by white noise (zero mean unit variance Gaussian process) at all the five floor level and integration scheme based on state space representation is implemented to obtain the time-history responses of the system at the sample rate of 128 Hz. White noise is added to the simulated acceleration data and the noise level is taken as 5% root mean square (RMS) noise-to-signal ratio.

Acceleration data with the duration of 60 s for the bottom three floors are used in modal analysis. The data are firstly transformed to TF coefficients using the STFT with the sliding (Hamming) window length of 1024 and window shift size of 2. SSPs are then detected based on the specified threshold (4 degrees) related to directional alignment of TF coefficients in Equation(5). For those SSPs, the real and imaginary parts of TF coefficients are collected together for the two-stepping clustering. Hierarchical cluster analysis is applied to SSP frequency values, classifying the SSPs into five groups with the frequency centroids at 0.95 Hz, 3.32 Hz, 7.09 Hz, 10.60 Hz and 12.66 Hz, respectively. The clustering algorithm in [35] is then implemented for each frequency group to classify TF coefficients. Outliers are automatically removed based on the criterion for cluster distribution, i.e. minimum sample number (e.g. >100), standard deviation of modal frequency values (<0.05) and standard deviation of point distance to cluster centroid (<0.05). Five clusters (i.e. 0.92 Hz, 3.39 Hz, 7.07 Hz, 10.70 Hz and 12.64 Hz) are derived with the corresponding mode shapes indicated in Figure 4. Dot markers represent estimated mode shape ordinates using the enhanced SCA method while the solid curves are the theoretical ones taken as the reference. Compared with the reference, the estimation results have the MAC values over 99.8%. For comparison, two other window functions (i.e. rectangular and Hann) are implemented in the STFT for TF transform. The achieved MAC values using either window function are high (over 99.6%) for all the five modes. Thus, the method is not sensitive to the window function chosen for STFT.

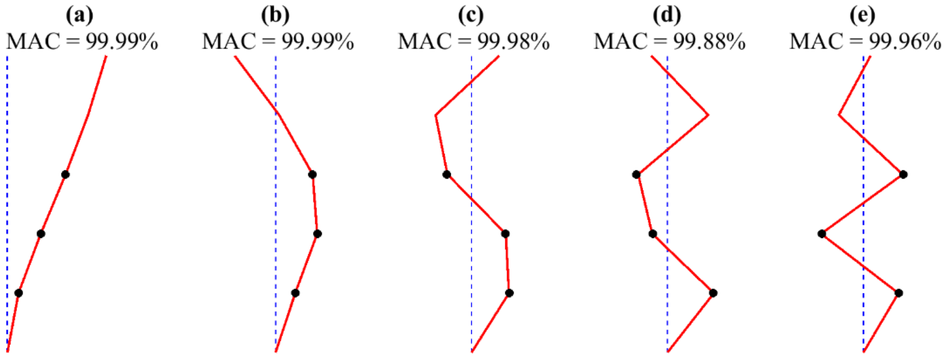

Figure 4 Mode shapes of a 5-DOF building system: solid curves represent the reference mode shapes in the simulation; and dot markers denote the modal shape ordinate estimated by the enhanced SCA method using three-channel acceleration data. Modal assurance criteria (MAC) compared with the reference mode shapes are given in subplot titles.

Given the mode shape matrix, the source TF representation is separated based on l^1 norm minimisation using an open source package SPGL1 [36,37] and then recovered to the time domain using inverse discrete Fourier transform. Figure 5 shows the estimated sources and the corresponding auto-spectral densities (ASD), indicating that the five sources are clearly identified using three-channel measurement.

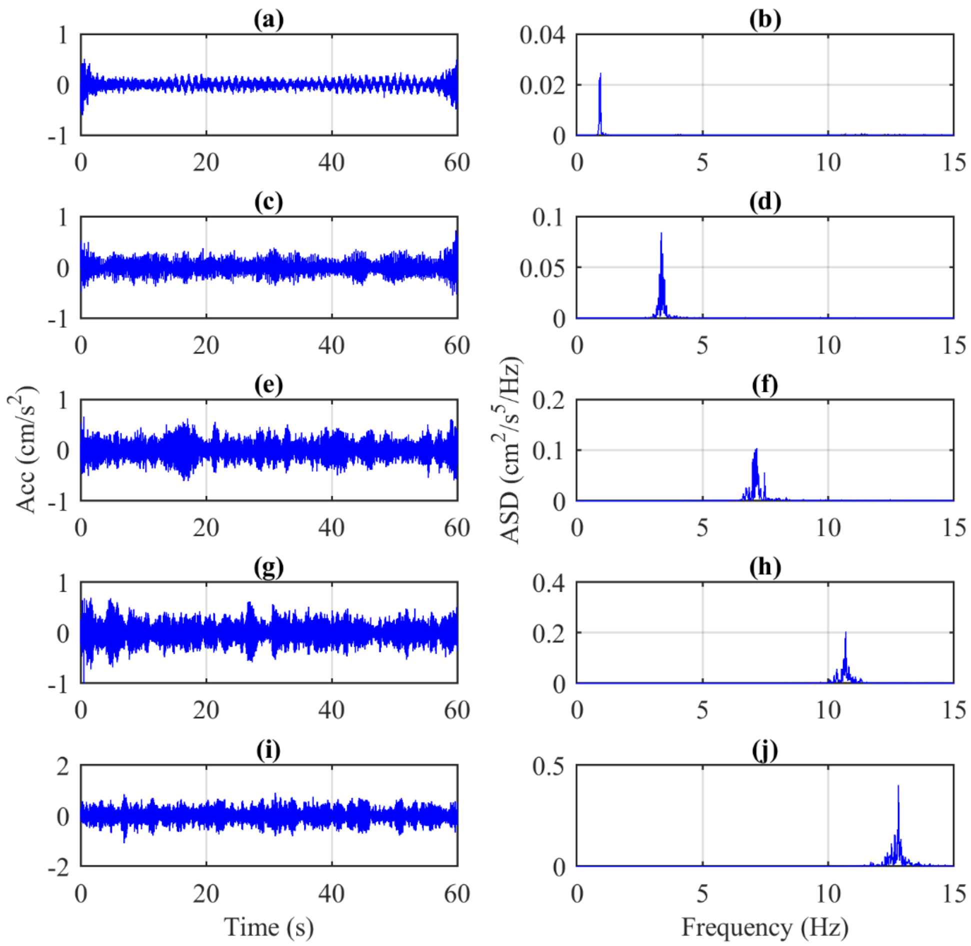

Figure 5 Five source signals recovered from three-channel measurement using the enhanced SCA method (the left column) and the corresponding auto-spectral densities (the right column).

TF transform representation is the necessary step in the SCA method for data sparsity. The simplest TF transform (i.e. STFT) is demonstrated to be effective in this numerical example and will be used with field data as described in sections 3 to 5, although there are other feasible alternatives e.g. wavelet packet transform [18] and quadratic TF transform [19].

Application to field test data collected from two bridges is described next. In section 3, the enhanced SCA method is firstly validated for OMA of a short-span road bridge using data collected by wired and wireless accelerometer sensors. The feasibility of the proposed method for analysing non-stationary vibration data is investigated in section 4 using the data from the same bridge under a heavy truck passage, while section 5 employing human-induced vibration data from a footbridge.

3 FIELD TEST ON A ROAD BRIDGE DURING NORMAL OPERATION

This section reports the validation study of the enhanced SCA method for OMA on a short-span road bridge. The extracted modal parameters using the new method are evaluated through comparison with the results by the NExT/ERA procedure [38]. NExT/ERA operational modal analysis procedure is chosen as the reference due to its long experience of use and availability in a custom software [39]. Essentially, section 3.1 introduces the test configuration on the bridge and demonstrates the measurement results. Modal analysis results using enhanced SCA are described in section 3.2 for mode shape estimation and in section 3.3 for modal parameter extraction.

3.1 Test configuration and measurement results

Station Road Bridge in Figure 6(a) is a steel girder bridge with 36 m span near Exeter St David's railway station. A modal test was performed on the bridge (also reported in [40]) using two types of sensors, wired Honeywell QA-750 accelerometers and APDM Opal^{TM} wireless inertial measurement units (IMUs).

The QA-750 accelerometers are DC-response devices with a resolution better than 1 μg and sensor noise floor better than 7 $\mu g/\sqrt{Hz}$ in 0-10 Hz band from manufacture data. The IMU Opal sensor includes a tri-axial accelerometer with the resolution of 240 μg and 730 μg for the sensing ranges of ±2 g and ±6 g, respectively and noise floor one or two orders of magnitude inferior to the QAs.

Sensors were arranged in six test points on the bridge, ¼ points (TP1 and TP4), mid-span (TP2 and TP5) and ¾ points (TP3 and TP6) of north and south sides, as indicated in Figure 6(b). With four QA accelerometers available, two runs of recordings were performed to cover all the six test points: two QAs were kept at the same locations (TP3 and TP5) while the other two were moved from TP1 and TP2 in the first run to TP4 and TP6 in the second run. Six Opal sensors were arranged in the six test points with one run of data recorded directly to the memory of each IMU. The sample rates for two sensing systems were both set as 128 Hz.

(a)

(b)

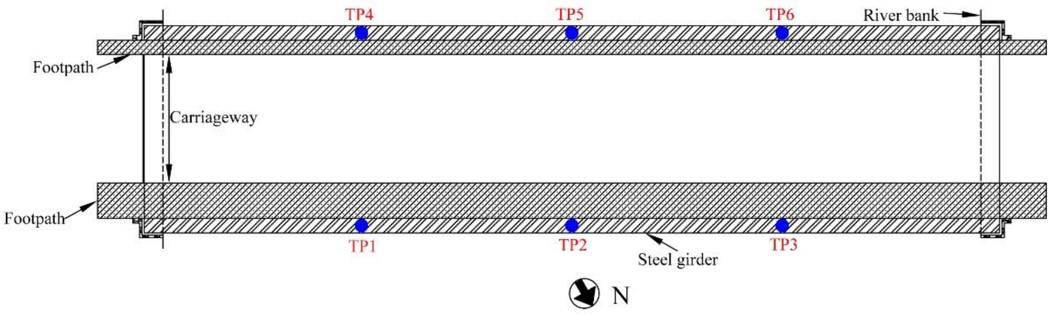

Figure 6 Bridge information and test point locations: (a) bridge elevation taken from the north side of the bridge; and (b) configuration of test points for accelerometer sensors.

The vertical acceleration signals from a 15-minute recording are truncated for the modal analysis. Vibration data collected by a QA accelerometer at TP3 in Run 1 are demonstrated in Figure 7 as an example. The experienced maximum acceleration reaches 0.43 m/s^2 and the auto-spectral density (ASD) indicates five modes lower than 18 Hz at approximately 3.1 Hz, 5.0 Hz, 7.5 Hz, 11.4 Hz and 13.7 Hz.

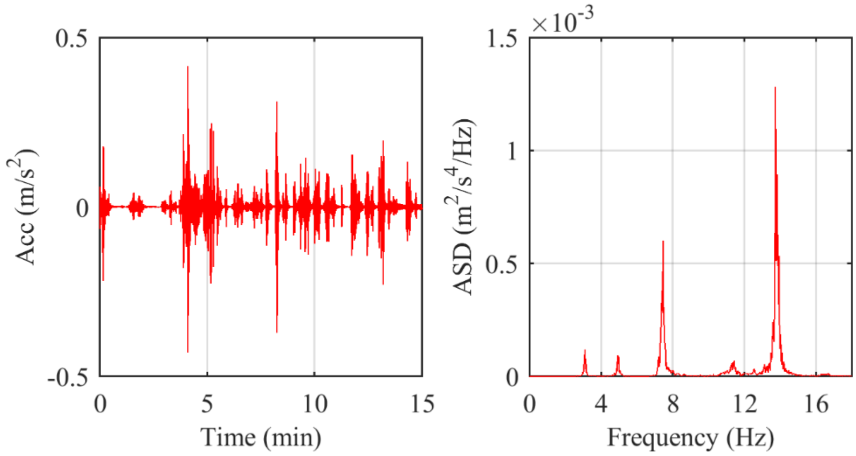

Figure 7 Time histories of vertical acceleration and the corresponding auto-spectral density (ASD) at test point TP3 in Run 1 by QA accelerometer.

3.2 Estimation of mode shapes by enhanced SCA method

The vibration data collected by QA and Opal sensors were analysed following the procedures of the enhanced SCA method in section 2.2. Firstly, the acceleration data were transformed to the TF domain by STFT using Hamming windows with the window length 14400 and the hop size 20 (i.e. the number of samples between the begin-steps of adjacent windows).

The second step is to estimate mode shapes using TF coefficients of the SSPs. The SSPs were detected based on directional alignment of the real and imaginary parts in TF coefficients using a threshold angle $\Delta\theta$. A smaller threshold angle $\Delta\theta$ corresponds to imposing a tougher requirement on the qualified SSPs, leading to a smaller number of SSPs. The specified angle $\Delta\theta$ for QA data is 2 degrees providing 45088 SSPs while the same value applied to Opal data leads to only 52 qualified SSPs and then failure of cluster analysis. A large value for $\Delta\theta$ (5 degrees) was taken to analyse the Opal data, providing 5544 qualified SSPs.

The two-step clustering results for the detected SSPs are shown in Figure 8: X and Y axes correspond to the frequency values (lower than 20 Hz) and the normalised TF coefficients at the test point TP3.

- The QA data in Run 1 are assigned to five groups shown in (a) with frequency centroids at 3.10 Hz, 4.98 Hz, 7.51 Hz, 11.41 Hz and 13.81 Hz, similar to observations from ASD plot in Figure 7 (b).
- Analysis results for QA data in Run 2 shown in (b) are similar to (a) but with slight difference in frequency centroid values.
- In (c), Opal data are assigned to four groups at 3.10 Hz, 4.90 Hz, 7.52 Hz and 13.71 Hz. For the SSPs in every cluster, the normalised TF coefficients (along the y axis) have larger variation ranges

compared with QA results possibly due to a more flexible criterion (higher threshold angle) on SSP detection. One cluster near 11.41 Hz that is visible from QA data is missed by Opal data.

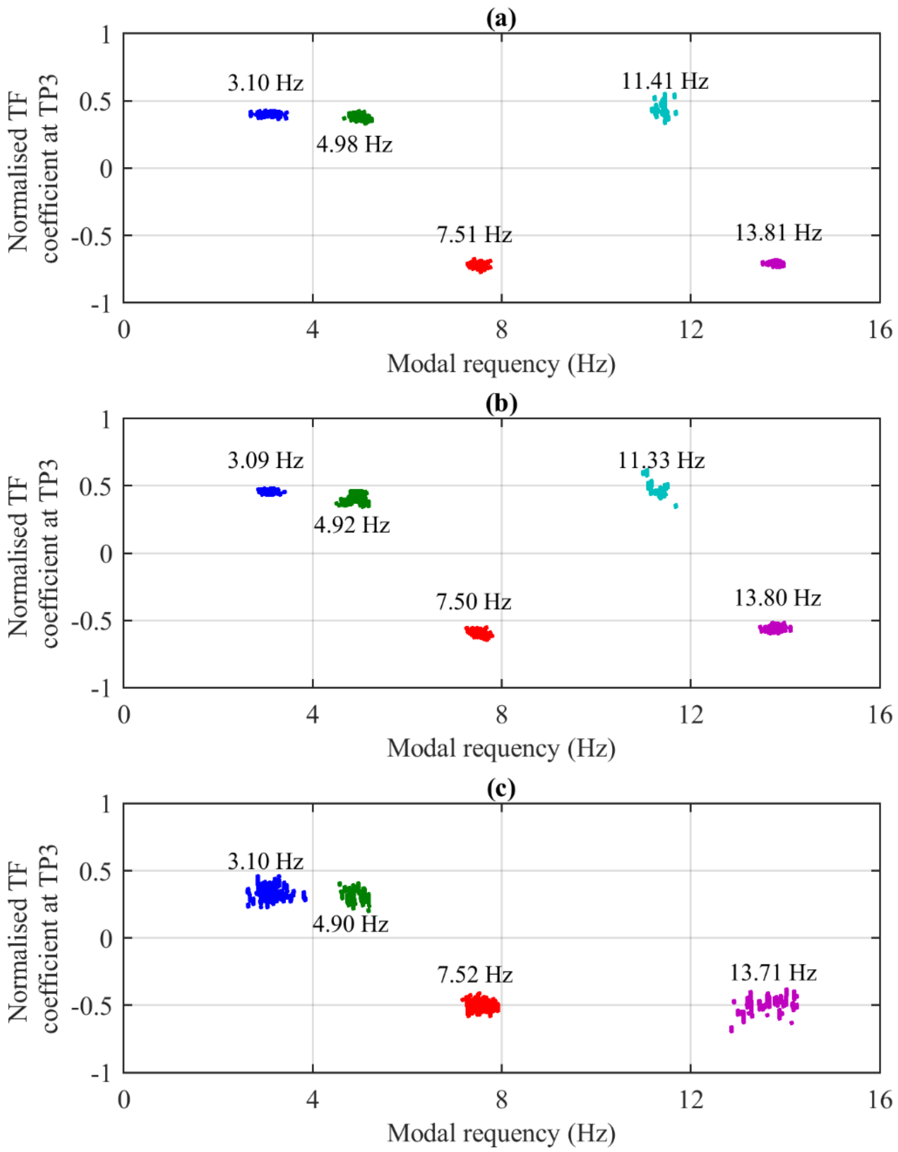

Figure 8 Clustering results about normalised TF coefficients from acceleration measurement: (a) clustering results for acceleration measurement in Run 1 by QA accelerometers; (b) clustering results for acceleration measurement in in Run 2 by QA accelerometers; and (c) clustering results for acceleration measurement by Opal IMUs.

For each cluster, the centroid of normalised TF coefficients represents directly one mode shape vector at test points. Mode shape vectors in two runs of QA measurement were merged based on the two reference test points with the results shown in the left column of Figure 9. In the figure, the red lines with circular markers and the black lines with ‘x’ shaped markers represent the mode shape ordinate of the two longitudinal sides of the bridge in the north and south, respectively. Subplots (b) and (e) indicate the first two torsion modes of the bridge while the other three are bending modes.

The mode shapes estimated from QA data using NExT/ERA procedures in [40] are taken as the reference to evaluate the estimation accuracy of the enhanced SCA method. For QA data, all the extracted five modes indicate high similarity with the reference and the modal assurance criteria (MAC) reach over 99.96%. In Run 1, four QA sensors were located at the three test points (i.e. ¼, ½ and ¾ span) in the north side, and the ½ span point in south. Based on four channel measurement, mode shape vectors of the third bending and first torsion modes (Figure 9(c) and (e)) are of high similarity and might be judged as one mode using traditional SCA method. The enhanced SCA method employs a two-step clustering procedure for automatic classification without any signal pre-processing and captures all the modes of interest accurately. It indicates that the proposed method is effective for the underdetermined case using limited sensors.

The mode shapes extracted from Opal IMU data are indicated in the right column of Figure 9. Compared with the reference, the estimation results have the MAC values over 99.2%. The third bending mode at approx. 11.41 Hz is missed due to a small number (< 100) of SSPs available in the adjacent frequency range.

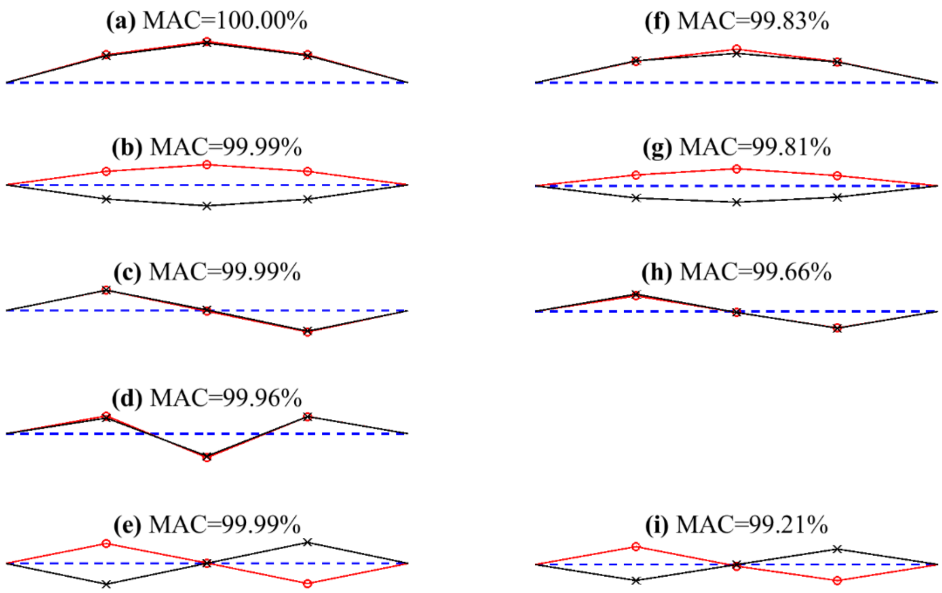

Figure 9 Estimated mode shapes by the enhanced SCA method: the left column corresponds to the first five modes of the bridge estimated from QA data (a-e); and the right column corresponds to the four modes of the bridge estimated from Opal IMU data (f-i). Dashed lines denote initial location of the bridge, solid lines with circular markers denote the mode shape ordinate of the north side of the bridge (TP1~3) and solid lines with 'x' shaped markers denote the mode shape ordinate of the south side of the bridge (TP4~6). The modal assurance criteria (MAC) compared with the mode shapes estimated by NExT/ERA method using QA measurement data [40] are given in the subplot titles.

3.3 *Extraction of modal parameters*

Given the estimated mode shapes, the TF representations of modal responses were separated based on l^1 norm minimisation using a MATLAB toolbox for the SPGL1 solver [41,42] and then reconstructed to the time domain by inverse STFT.

QA acceleration data covering a free decay period were truncated for modal parameter estimation with the duration of 22 seconds, presenting in the left column of Figure 10. The modal responses were separated from the measurement signals based on the estimated mode shapes. Due to the existence of very similar mode shapes that are indistinguishable using four test points, the output of modal responses might carry two or more frequency components and are not necessarily single degree-of-freedom signals. Hence a band-pass filter with the bandwidth of 2 Hz around the frequency value of a cluster centroid (in section 3.2) was applied to the modal response with the results shown in the right column of Figure 10.

The modal frequencies were estimated by the peak-picking method from the auto-spectral densities of the filtered modal responses. The damping ratios were derived from the free decay parts using the logarithmic decrement method and the fitted envelopes are indicated as red lines in modal response plots. The estimation results of modal parameters are given in Table 1 compared with those by the NExT/ERA method in [40]. The frequency estimates match very well with difference within 0.3%. Although the estimated damping ratios are much smaller than the values by the NExT/ERA method, the estimates from free-decay signals in this study could be reliable since the fitted envelops of damped vibration curves in Figure 10(e) to (i) match very well with the actual ones.

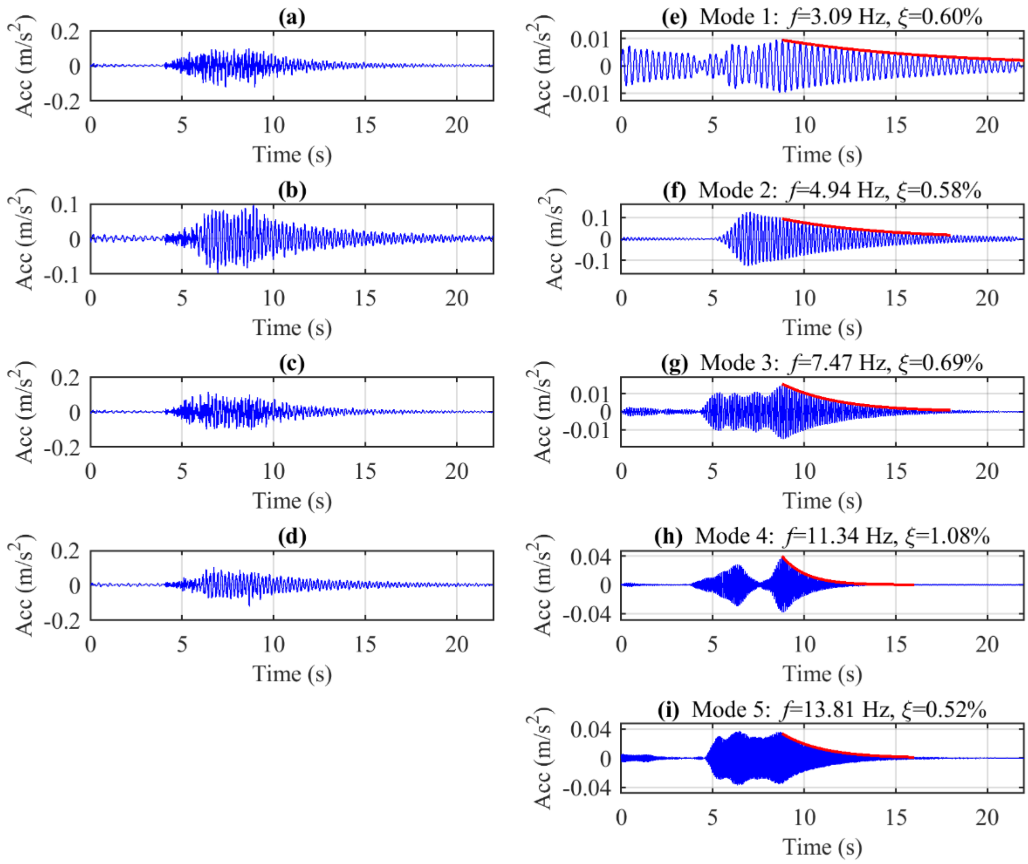

Figure 10 Truncated 22 s signals of QA acceleration measurement in Run 1 and the corresponding modal response signals separated by l^1 norm minimisation: the left column (a-d) corresponds to acceleration measurement by four QA accelerometers at test locations TP1, TP2, TP3 and TP5; and the right column (e-i) corresponds to the modal response signals separated by the SCA method after implementing a band-pass filter with the bandwidth of 2 Hz around the modal frequencies. Logarithmic decrement method is used for damping ratio estimation with the fitted envelops (red lines) indicated in modal response plots (in the right column).

Table 1 Modal frequencies (f) and damping ratios (ξ) of the first five modes estimated by the enhanced SCA method and the NExT/ERA procedure [40] using QA data

Mode number	**Enhanced SCA**		**NExT/ERA**	
	F (Hz)	ξ	f (Hz)	ξ
1	3.09	0.60%	3.10	1.75%
2	4.94	0.58%	4.94	0.99%
3	7.47	0.69%	7.47	1.07%
4	11.34	1.08%	11.35	1.87%
5	13.81	0.52%	13.78	0.84%

After validating the enhanced SCA method for the OMA of ambient vibration of a road bridge, the proposed method is applied to modal identification of truck-induced non-stationary vibration data for the same bridge in section 4 and then for pedestrian-induced vibration data of a footbridge in section 5.

4 FIELD TEST ON A ROAD BRIDGE DURING HEAVY TRUCK PASSAGE

Some of the classic OMA methods like the NExT and SSI impose the assumption of stationary excitation process and thus are challenging for analysing non-stationary signals such as truck-induced and human-induced vibrations. The SCA-based method is feasible in this case because the underlying assumption for the SCA is essentially geometrical about the sparsity of sources [31].

In this section, the enhanced SCA method is implemented for the modal identification of non-stationary signals recorded on a road bridge (the same bridge as in section 3) under heavy truck passages. Section 4.1 introduces the test configuration on the bridge and demonstrates the measurement results while section 4.2 presents the estimated results of mode shapes using the enhanced SCA method. The step of modal parameter estimation is not presented in this section as it is very similar to the content in section 3.3.

4.1 Test configuration and measurement results

The truck used in the test had a total weight of 32 t with four axles shown in Figure 11(a). Sensors used for recording consisted of four QA accelerometers located at the ¼ point (TP1), mid-span points (TP2 and TP5), and ¾ point (TP3) in Figure 11(b). The sample rate was set as 256 Hz. The truck passed the bridge, without stopping, from the west to the east using the north lane in Run 1 and from the east to the west using the south lane in Run 2.

(a)

(b)

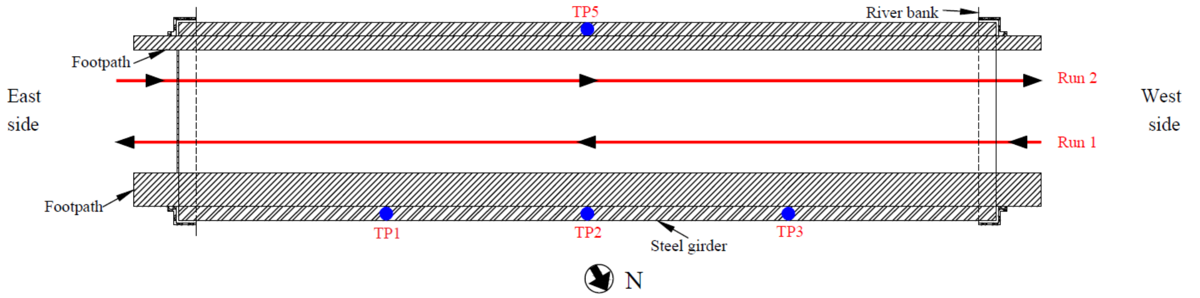

Figure 11 Truck information and test point locations: (a) the truck used in the test; and (b) locations of four QA accelerometers and truck passage routes in two runs.

Vibration data during the truck passages were truncated for the analysis. The time series data at TP3 in two runs are shown in Figure 12 (a) and (c) and the maximum acceleration experienced was 0.33 m/s^2 and 0.70 m/s^2, respectively. Auto-spectral densities of the signals shown in (a) and (c) are estimated using the Welch's method and the results are shown in Figure 12(b) and (d) respectively. Modes that received more energy in Run 1 are the second bending mode at 7.5 Hz and the second torsion mode at 13.8 Hz while the first torsion mode at 4.95 Hz becomes more apparent in Run 2. This is likely related to the fact that during Run 2 the truck was closer to the edge of the deck than in is in Run 1 due to the narrower footpath on the south side of the bridge. Two or three peaks with high energy are observed near 13.8 Hz that indicate the non-stationary and time-varying feature of the vibration signals.

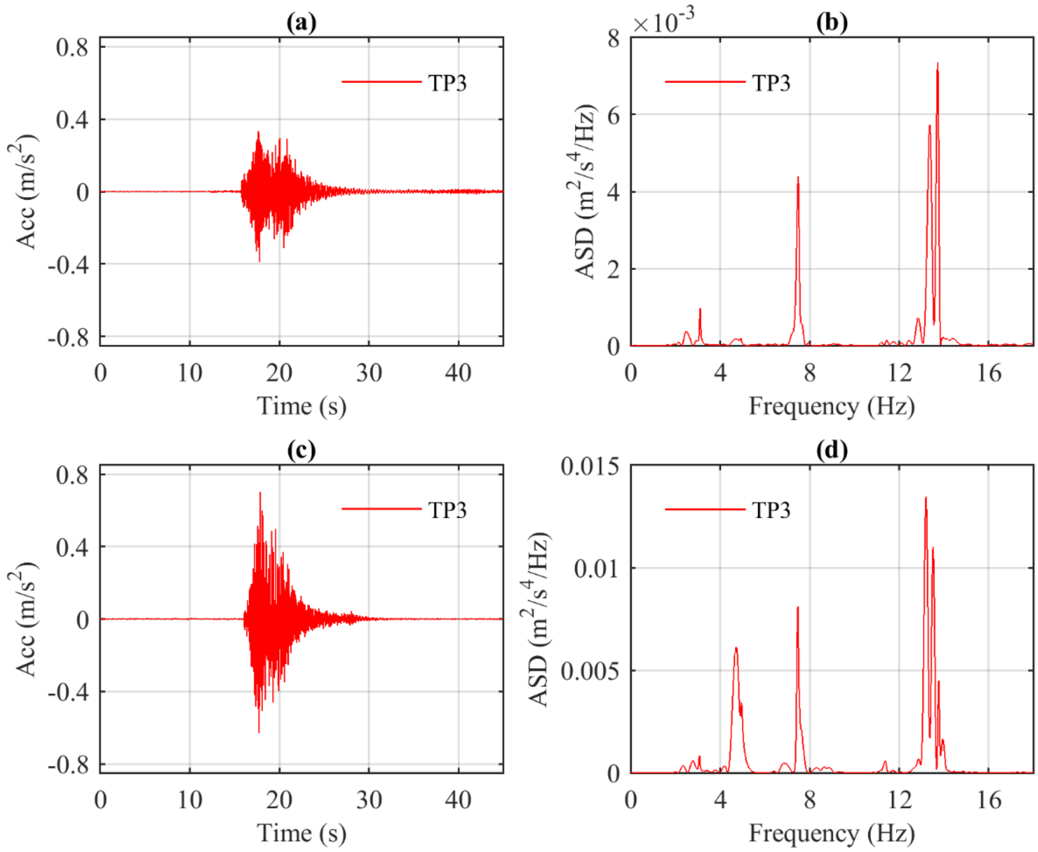

Figure 12 Vertical acceleration measurement at TP3 during the truck passages in two runs and the corresponding auto-spectral densities: (a) acceleration measurement recorded when the truck passed the bridge from the west to the east in Run 1; (b) auto-spectral densities of acceleration data in (a); (c) acceleration measurement recorded when the truck passed the bridge from the east to the west in Run 2; and (d) auto-spectral densities of acceleration data in (c).

4.2 Estimation of mode shapes by enhanced SCA method

Mode shapes of the bridge were estimated following the procedures of the enhanced SCA method in section 2.2. The TF transform applied to vibration data is STFT using Hamming windows with the window length 5760 and the hop size 2. The threshold angle $\Delta\theta$ for SSP detection was taken as 2 degrees, same as in section 3.2.

Table 2 provides the estimation results of modal frequencies and also the MAC values compared with the references that are mode shapes estimated in section 3 using QA data.

- For the first bending mode initially at 3.09 Hz, three mode shapes in Run 1 at 2.11 Hz, 2.57 Hz and 3.09 Hz are observed reaching high MAC values (>99.5%) compared with the reference. In Run 2, four modes at 2.29 Hz, 2.59 Hz, 3.08 Hz and 3.27 Hz are identified with similar mode shapes as the reference. Initially the appearance of multiple frequencies that have the same apparent mode shape is surprising. However, it is to do with the fact that when the truck is on the bridge, the frequencies of this coupled system consisting of the vehicle and the bridge can vary with truck position, resulting in a non-stationary vibration signal. This phenomena is not the focus of this paper so is not discussed further here, but has been reported in detail in [43].
- For the first torsion mode initially at 4.94 Hz, the mode shape estimates at 4.53 Hz from the data in Run 1 has the MAC of 95.87%. In Run 2, two modes at 4.16 Hz and 4.81 Hz are identified with the MAC values of 99.19% and 99.97%, respectively. These modes are demonstrated in Figure 13. In Run 1 when the truck passed from the west to the east using the north lane of the carriageway, the modal displacement in the north side (TP1~3) apparently decreased while that for TP5 in the south side increased slightly. Mode shape changes in Run 2 are less obvious.
- The information of the other three modes lower than 15 Hz is given in Table 2. The 3rd bending mode is missed when analysing the vibration data in Run 2. The MAC values between the identified mode shapes and the reference are higher than 98.8%.

Table 2 Modal frequency estimates during truck passages and the MAC values compared with the mode shapes estimated in section 3 using ambient vibration data recorded by QA accelerometers.

Mode No.	Test runs	Modal Frequency (Hz)	MAC
1st bending	Reference	3.09	--
	Run 1	2.11	99.81%
		2.57	99.70%
		3.09	99.99%

	Run 2	2.29	98.98%
		2.59	99.90%
		3.08	99.99%
		3.27	99.56%
1st torsion	Reference	4.94	--
	Run 1	4.53	**95.87%**
	Run 2	4.16	99.19%
		4.84	99.97%
2nd bending	Reference	7.47	--
	Run 1	7.52	99.96%
	Run 2	7.45	99.26%
3rd bending	Reference	11.34	--
	Run 1	11.36	99.68%
	Run 2	Not available	Not available
2nd torsion	Reference	13.81	--
	Run 1	13.75	99.35%
	Run 2	13.23	98.86%
		13.56	99.67%

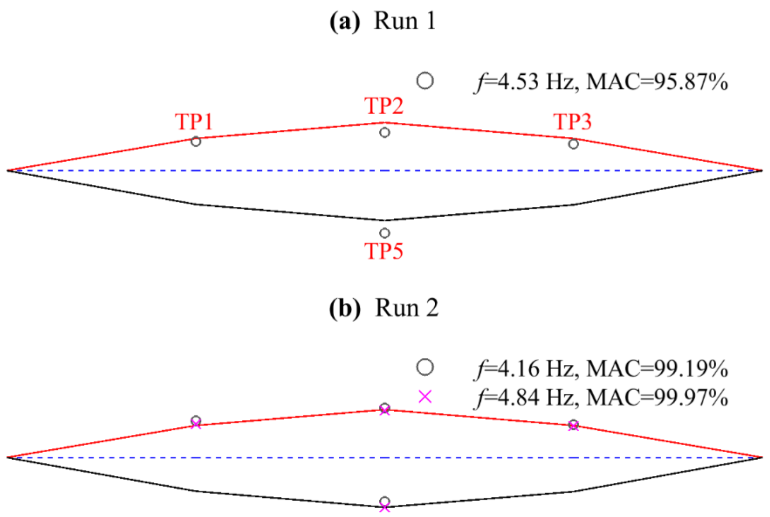

Figure 13 Estimation results of the first torsion modes during truck passages in Run 1 and Run 2. Dashed lines denote initial location of the bridge; two solid lines denote the reference mode shape ordinate of the north and south sides of the bridge estimated using ambient vibration data of QA accelerometers in Section 3. Circular and 'x' shaped markers denote the mode shape ordinate estimated using vibration data during truck passages; and the corresponding modal frequencies and MAC values compared with the reference mode shapes are given in the legends.

Analysis results indicate that the enhanced SCA method is capable of analysing non-stationary vibration signals, i.e. identifying accurately bridge mode shapes and capturing additional modes due to changes of system properties. The procedures are intended to identify such changes while their interpretation requires structural engineering expertise supported by numerical modelling and further investigations.

5 FIELD TEST ON A FOOTBRIDGE

In this section, the enhanced SCA method is implemented for modal identification of vibration signals recorded on a cable-stayed footbridge. There are some challenges of implementing classical OMA methods e.g. NExT/ERA and SSI to capture modal information completely for this bridge as it has several closely-spaced modes and experiences high energy only in frequency components close to pedestrian pacing rates. Section 5.1 introduces the bridge and the test configuration and then demonstrates the measurement results, while section 5.2 and 5.3 presents the estimated results of mode shapes and modal frequencies using the enhanced SCA method.

5.1 Test configuration and measurement results

Baker Bridge, shown in Figure 14, is a cable-stayed footbridge with the span length 109 m in Exeter, UK. The bridge links Digby & Sowton railway station in the north to the Sandy Park Stadium in the south that is the home ground of Exeter Chiefs Rugby Club. The bridge has six vertical modes lower than 3.5 Hz [44] and thus experiences considerable dynamic response to pedestrian traffic.

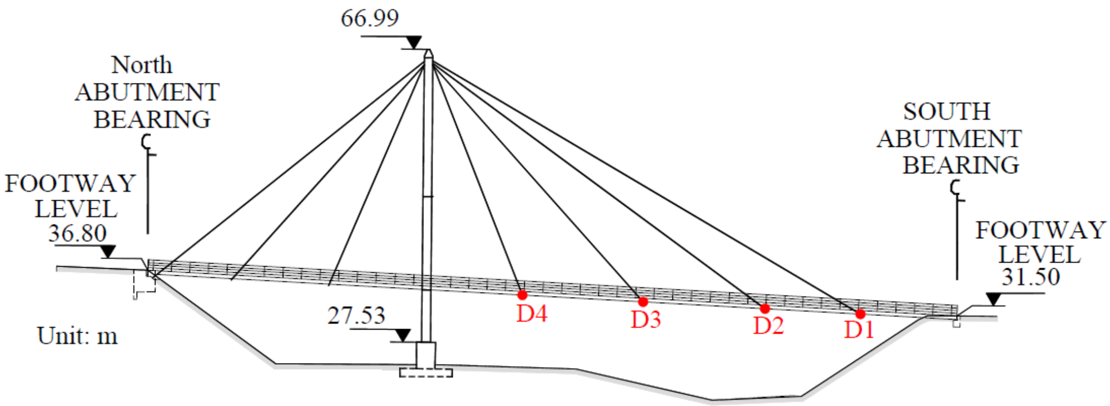

(a)

(b)

Figure 14 Bridge information and sensor locations: (a) bridge elevation and locations of four Opal IMUs at D1 to D4 in the southwest side of the bridge; and (b) west elevation of the south span of the bridge at 14:28:30 PM from a recorded video file on the test day.

Four APDM Opal^{TM} IMU sensors were installed on the south span adjacent to the west parapet at D1 to D4, as shown in Figure 14(a) on a match day. The match kick-off time was 15:00 PM. The sample rate was set as 128 Hz.

Vibration data from 14:20 PM to 15:20 PM were truncated for modal identification. The vertical acceleration measurement shown in Figure 15(a) indicates that the bridge became very quiet after the match kick-off at 15:00 PM. Auto-spectral densities estimated using the Welch's method are shown in Figure 15(b). The two modes with the frequencies close to the normal walking pace (2 Hz) are the strongest and most obvious.

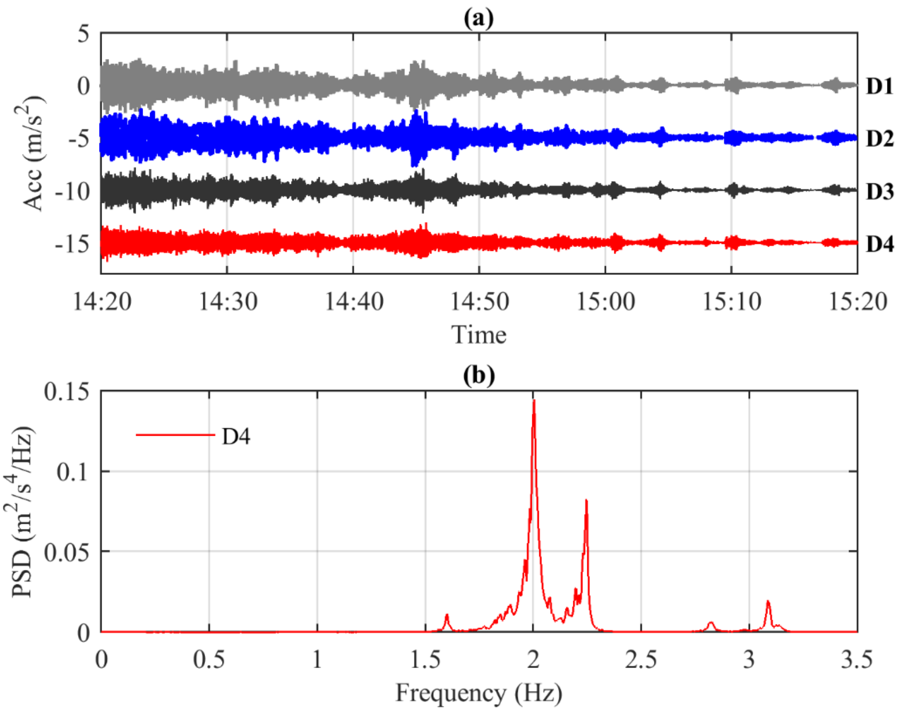

Figure 15 Acceleration measurement by four Opal IMUs in the vertical direction and the corresponding auto-spectral densities: (a) acceleration measurement from 14:20 PM to 15:20 PM; and (b) the auto-spectral densities of acceleration measurement at D4 in (a).

5.2 Estimation of mode shapes by enhanced SCA method

Following the two-step clustering described in section 2.2, mode shapes and frequencies were extracted from each cluster centroid of normalised TF coefficients. The threshold angle $\Delta\theta$ for SSP detection was taken as 5 degrees, same as for Opal measurement in section 3.2.

Figure 16 demonstrates the first six mode shapes estimated by the enhanced SCA method together with the reference that is derived from the previous ambient modal test [44] using NExT/ERA procedures. In this ambient modal test, six wireless accelerometer sensors were used to record bridge vibrations. Two sensors were kept at the same points as the reference while the other four were 'roved' over the remaining 30 test points (covering bridge two sides) in several recordings. Mode shape and modal frequency information for the first six modes have been demonstrated in [44] and now are re-interpreted here as the reference: Solid and dashed curves correspond to modal shape ordinate of the west and east sides of the bridge.

The dot markers denote the modal shape ordinate at D1~D4 on the west side of the bridge estimated by the enhanced SCA method using Opal IMU data. The first five mode shape estimates using the enhanced SCA method match well with the reference with the MAC values over 99.5% while the MAC value for the six mode is slightly lower (98.19%).

In this example, mode shape vectors for the third and fourth bending modes (Figure 16(c) and (d)) are of high similarity based on the four channel measurement (D1-4) and should be challenging to be distinguished via traditional SCA method. The demonstration example validated again the feasibility of the enhanced SCA method for the underdetermined case using limited sensors.

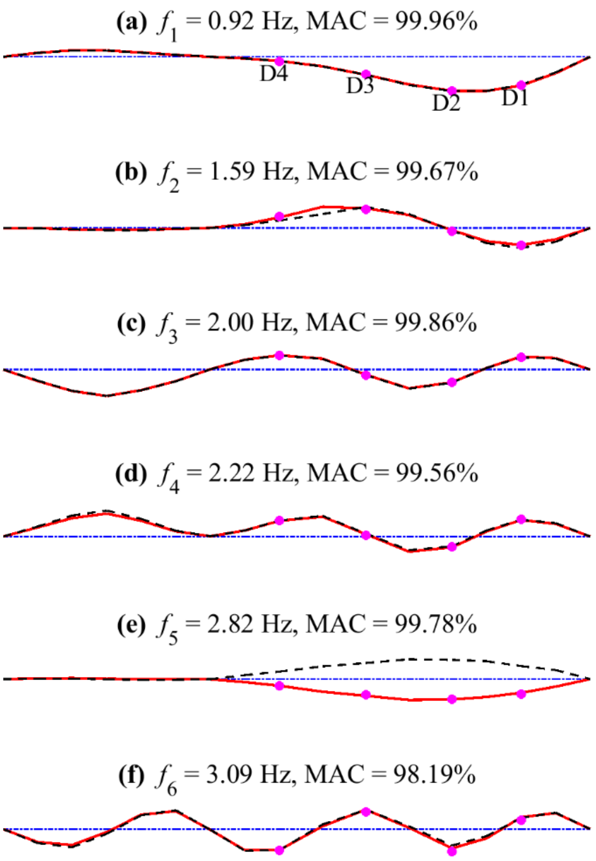

Figure 16 Estimated mode shapes by the enhanced SCA method together with reference mode shapes of the bridge: solid and dashed curves denote the reference mode shape ordinate from a previous modal test using the NExT/ERA method [44] in the west and east sides of the bridge, respectively; and dot markers denote the modal shape ordinate estimated by the enhanced SCA method using acceleration data (in Figure 15(a)) from four Opal IMUs located at the southwest side of the bridge. Estimates by the enhanced SCA method including modal frequencies and modal assurance criteria (MAC) compared with the reference mode shapes are given in subplot titles.

5.3 Extraction of modal parameters

Based on vibration signals involving some periods with a crowd of pedestrians shown in Figure 14(b), the mode shape estimates in Figure 16 still have good match with the results in a previous ambient modal test. This indicates that the non-stationary feature of human-induced vibrations in this study is not apparently reflected in mode shape changes.

To investigate the time-varying characteristics, two time intervals of the separated modal responses with the duration of two minutes were truncated for modal parameter estimation when the bridge was occupied by a few pedestrians and a crowd, respectively. The raw acceleration measurement at D4 during these two selected periods is shown in Figure 17(a) and (c). The experienced maximum acceleration reaches 0.29 m/s^2 and 1.31 m/s^2, respectively and the strongest mode is both at 2 Hz, where with the auto-spectral density for the crowd is almost an order of magnitude stronger.

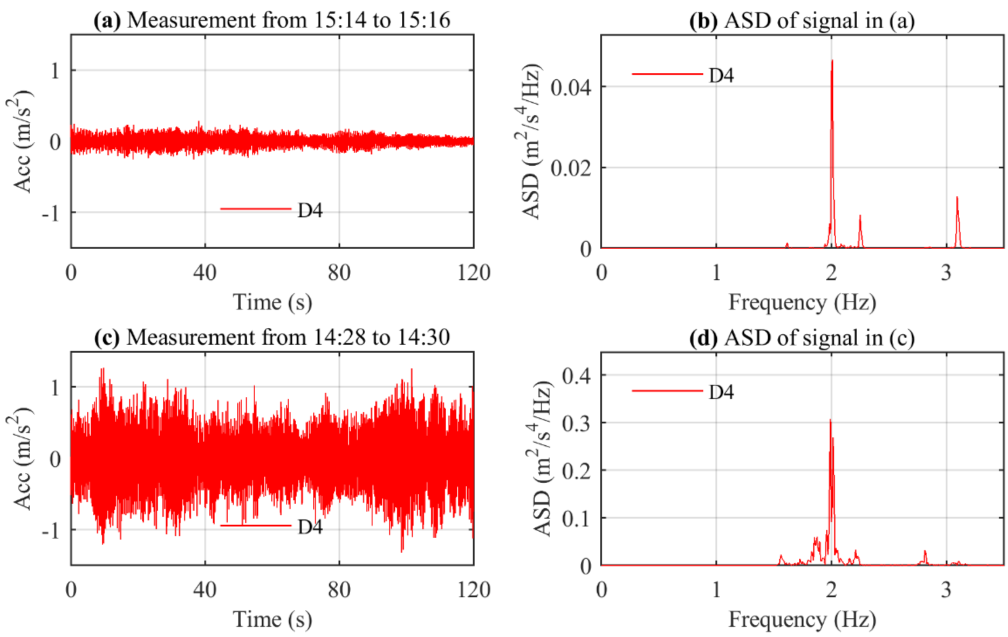

Figure 17 Acceleration measurement at D4 during two time intervals (when the bridge was occupied by a few pedestrians and a crowd, respectively) and the corresponding auto-spectral densities: (a) vertical acceleration measurement at D4 from 15:14 to 15:16; (b) auto-spectral densities of the acceleration signal in (a); (c) vertical acceleration measurement at D4 from 14:28 to 14:30; and (d) auto-spectral densities of the acceleration signal in (c).

Figure 18 and Figure 19 provide the separated modal responses and the corresponding auto-spectral densities recovered from the two time intervals.

For the estimated results in the first time interval (Figure 18), the modal responses are close to single-degree-of-freedom signals except in (a) for the first bending mode (at approximately 0.94 Hz) where some frequency components near 2.1 Hz (slightly deviated from the third bending mode frequency of 2.0 Hz) also contain considerable energy.

For the estimated results in the second time interval (Figure 19), clear peaks near dominant modal frequencies are indicated in the auto-spectral density plots of the third, fifth and sixth modal responses. The first, second and fourth modal responses involve considerable energy in the frequency components between 1.8 Hz and 2.1 Hz that are probably due to the excitations of walking pedestrians.

The modal frequencies were extracted from the auto-spectral density plots by the peak-picking method. As a comparison, the acceleration signals were also analysed directly by the covariance-driven SSI method for modal frequency estimation. The variables were set as 180 points in the covariance function and maximum order of 80 poles. Table 3 provides modal frequency estimates by the two methods as well as a reference from the previous ambient modal test [44] using NExT/ERA method. Observations in Table 3 show that,

- The enhanced SCA method identifies all the first six modes lower than 3.5 Hz from vibration data in either quiet or busy periods. The SSI method fails to capture some modes (e.g. 0.94 Hz and 3.09 Hz) even when weighting algorithms (e.g. Canonical Variate Analysis, Principal Components or Unweighted Principal Components) are considered for performance improvement. It is possibly due to the low-energy in the adjacent frequency ranges as shown in Figure 17(b) and (d). The enhanced SCA method is feasible for the low-energy modes because the information used for cluster analysis is the set of unit vectors of normalised TF coefficients, and their scales are neglected.
- Compared with the previous ambient modal test results, the modal frequency estimates in the first time interval match very well, while in the second time interval the first two modal frequencies are apparently reduced due to heavy pedestrian occupation.

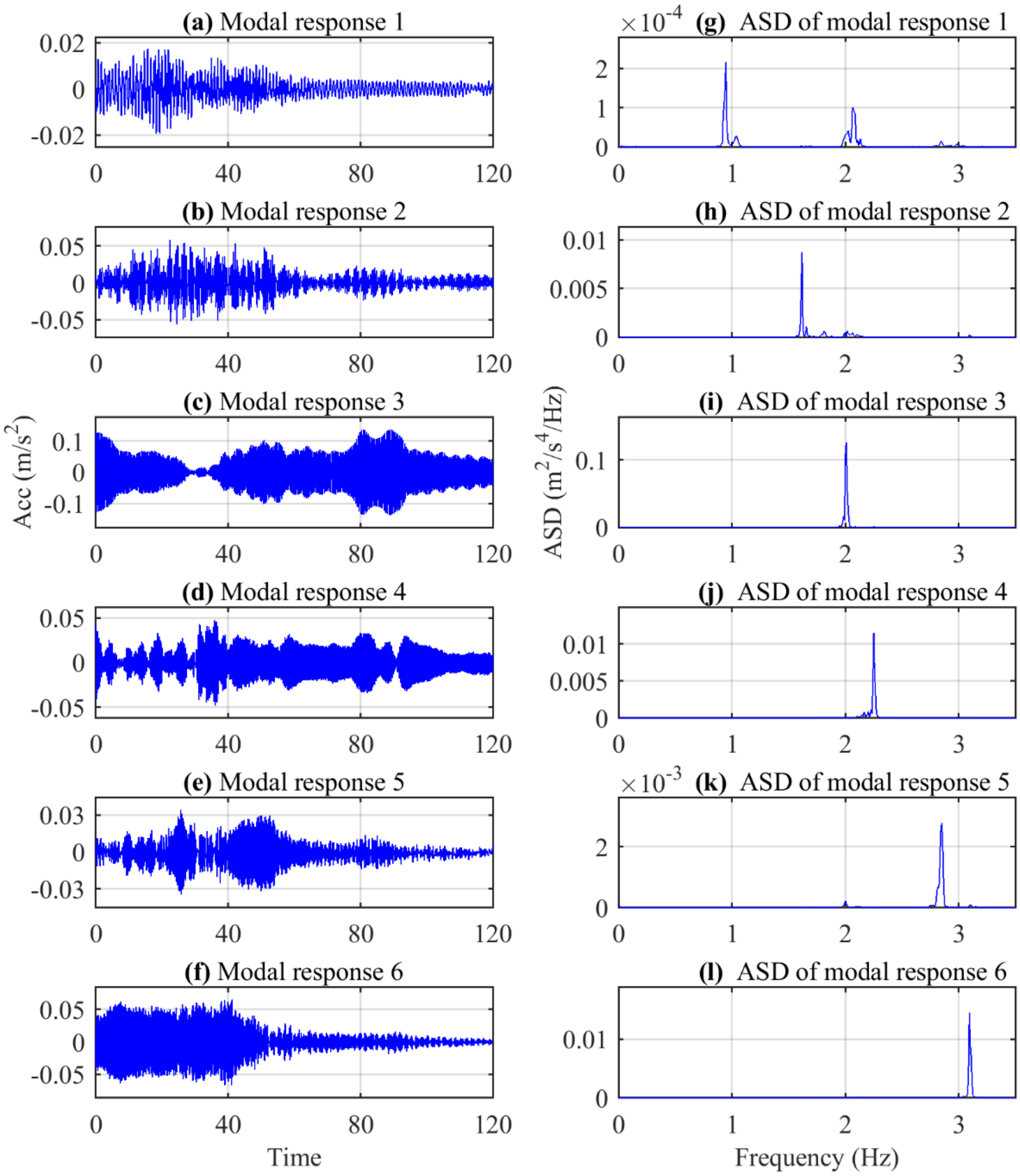

Figure 18 Modal response signals and the corresponding auto-spectral densities in the first time interval when the bridge was occupied by a few pedestrians: the left column (a-f) corresponds to the modal response signals separated by the SCA method; and the right column (g-l) corresponds to the auto-spectral densities of the signals in the left column.

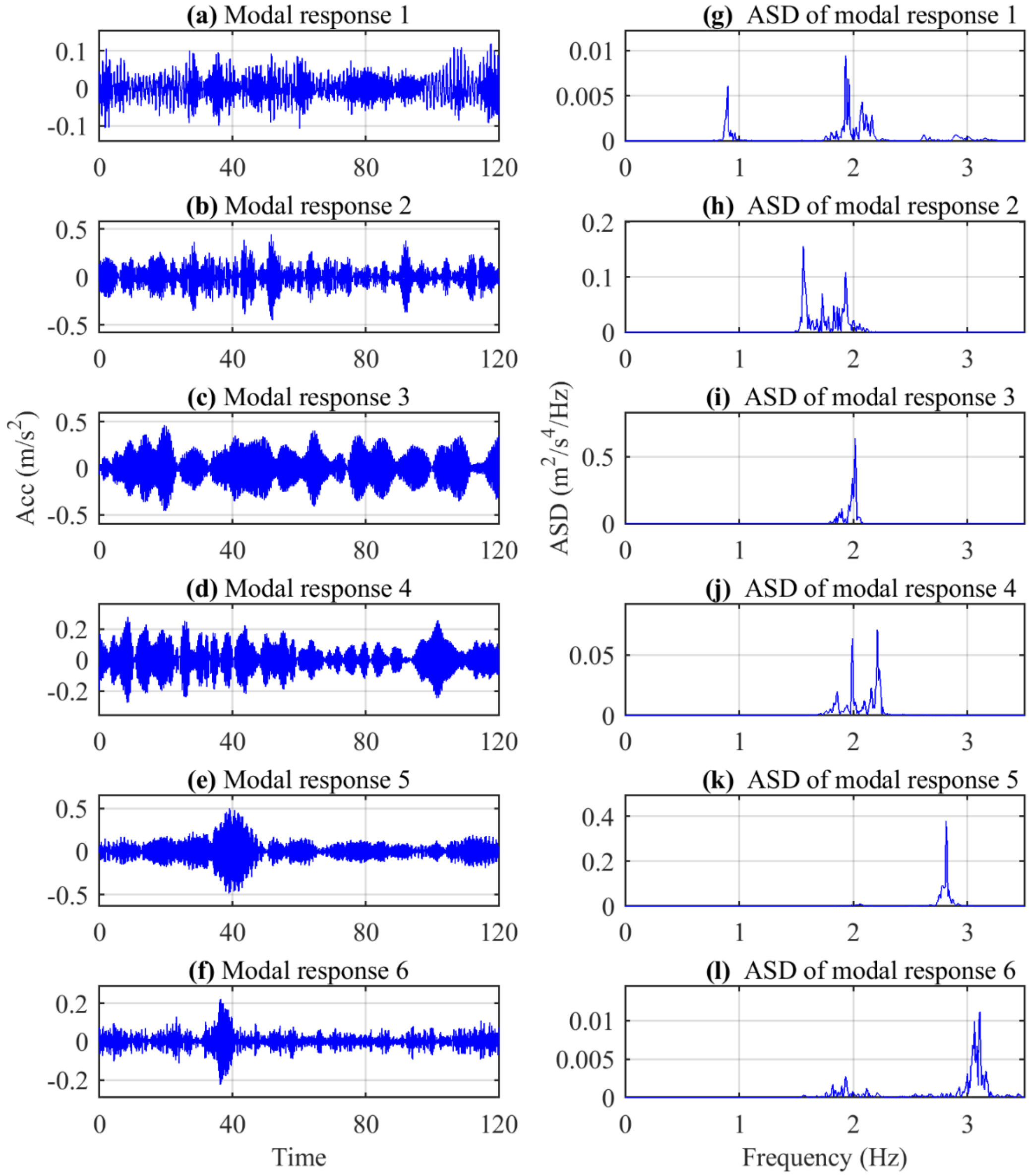

Figure 19 Modal response signals and the corresponding auto-spectral densities in the second time interval when the bridge was occupied by crowds of pedestrians: the left column (a-f) corresponds to the modal response signals separated by the SCA method; and the right column (g-l) corresponds to the auto-spectral densities of the signals in the left column.

Table 3 Estimated modal frequencies of Baker Bridge: the 2^{nd} column denotes modal frequencies estimated in a previous ambient modal test [44] by NExT/ERA method; the 3^{rd} to 4^{th} columns represent the modal frequencies estimated from acceleration data in the first time interval by the enhanced SCA and SSI methods; and the 5^{th} to 6^{th} columns represent the modal frequencies estimated from acceleration data in the second time interval by the enhanced SCA and SSI methods.

Modal frequency (Hz)	Previous modal test	Time interval 1		Time interval 2	
		By enhanced SCA	By SSI	By enhanced SCA	By SSI
Mode 1	0.94	0.95	--	0.90	--
Mode 2	1.62	1.62	1.60	1.56	1.56
Mode 3	2.00	2.01	2.01	2.02	1.98
Mode 4	2.24	2.25	2.25	2.21	--
Mode 5	2.84	2.85	2.83	2.81	2.81
Mode 6	3.08	3.09	3.10	3.11	--

Results indicate the enhanced SCA method provides accurate estimates of mode shapes and frequencies for human-induced vibrations and is capable to capture low-energy modes that is infeasible by SSI method. The non-stationary characteristics are reflected in the reconstructed modal responses with time-varying modal frequencies and possibly including the components of pedestrian excitations.

6 CONCLUSIONS

This study proposes an enhanced SCA method for structural modal identification. Through direct application to field test data, the method is validated to be capable of providing comparative results about modal parameters from ambient vibration data as the classic OMA method NExT/ERA. Compared with traditional SCA method, the proposed method has the advantage of accurately identifying highly similar modes that is beneficial for structural modal testing using limited sensors.

The enhanced SCA method has no assumption regarding the nature of excitation forces and is validated to be effective for analysing non-stationary signals including vehicle-induced and human-induced vibrations. For vehicle-induced vibrations, small changes in mode shapes and modal frequencies due to the time-varying feature can be captured. For human-induced vibrations, the mode shape changes are negligible in this study while the recovered modal response signals are non-stationary, reflecting small changes of modal frequencies as well as the components of pedestrian excitations. The proposed method could identify easily the low-energy and closely-spaced modes, indicating better performance than the SSI method.

Compared with other OMA methods, the enhanced SCA method in this study has less dependence on parameter selection and potentially fits the requirements of automatic modal identification on field test data.

7 ACKNOWLEDGEMENTS

We would like to acknowledge the Bridge Section of The Engineering Design Group of Devon County Council for permission to use their bridge and for assistance they provided. The third author gratefully thanks the funding from the People Programme (Marie Curie Actions) of the European Union’s Seventh Framework Programme (FP7/2007-2013) under grant agreement n° 330195. Also thanks to Mateusz Bocian and James Bassitt for support in the field testing on Station Road Bridge; thanks to Vincent Ao and Jose Capilla for support in the field testing on Baker Bridge. Finally, the authors would like to thank the two anonymous reviewers for their constructive comments.

8 DECLARATION OF CONFLICTING INTERESTS

The authors declare that there is no conflict of interest.

9 REFERENCES

[1] L. Zhang, R. Brincker, P. Andersen, An Overview of Operational Modal Analysis : Major Development and Issues: Major Developments of OMA, in: 1St Int. Oper. Modal Anal. Conf., Copenhagen, Denmark, 2005: p. 12.

[2] G.H. James III, T.G. Carne, Lauffer, J. P., J.P. Lauffer, The Natural Excitation Technique (NExT) for Modal Parameter Extraction From Operating Wind Turbines, 1993. doi:SAND92-1666.

[3] J.-N. JUANG, R.S. PAPPA, An eigensystem realization algorithm for modal parameter identification and model reduction, J. Guid. Control. Dyn. 8 (1985) 620–627. doi:10.2514/3.20031.

[4] B. Peeters, G. De Roeck, Reference-based stochastic subspace identification for output-only modal analysis, Mech. Syst. Signal Process. 13 (1999) 855–878. doi:10.1006/mssp.1999.1249.

[5] C. Gontier, M. Smail, P.E. Gautier, A time domain method for the identification of dynamic parameters of structures, Mech. Syst. Signal Process. 7 (1993) 45–56. doi:10.1016/0888-3270(93)90004-G.

[6] R. Brincker, L. Zhang, A. Palle, Modal Identification from Ambient Responses using Frequency Domain Decomposition, in: Proc. 18th Int. Modal Anal. Conf., San Antonio, Texas, USA, 2000. http://scholar.google.com/scholar?hl=en&btnG=Search&q=intitle:Modal+Identification+from+Ambient+Responses+using+Frequency+Domain+Decomposition#0.

[7] N.E. Huang, Z. Shen, S.R. Long, M.C. Wu, H.H. Shih, Q. Zheng, N.-C. Yen, C.C. Tung, H.H. Liu, The empirical mode decomposition and the Hilbert spectrum for nonlinear and non-stationary time series analysis, Proc. R. Soc. (1998) 903–995.

[8] N.E. Huang, Z. Shen, S.R. Long, A NEW VIEW OF NONLINEAR WATER WAVES: The Hilbert Spectrum, Annu. Rev. Fluid Mech. 31 (1999) 417–457. doi:10.1146/annurev.fluid.31.1.417.

[9] N.E. Huang, M.-L.C. Wu, S.R. Long, S.S.P. Shen, W. Qu, P. Gloersen, K.L. Fan, A confidence limit for the empirical mode decomposition and Hilbert spectral analysis, Proc. R. Soc. A Math. Phys. Eng. Sci. 459 (2003) 2317–2345. doi:10.1098/rspa.2003.1123.

[10] N.E. Huang, Z. Wu, A review on Hilbert-Huang transform: Method and its applications to geophysical studies, Rev. Geophys. 46 (2008) RG2006. doi:10.1029/2007RG000228.

[11] Z. Wu, N. Huang, Ensemble Empirical Mode Decomposition: a Noise-Assisted Data Analysis

Method, Adv. Adapt. Data Anal. 1 (2009) 1–41. doi:doi: 10.1142/S1793536909000047.

[12] N. Rehman, D.P. Mandic, Multivariate empirical mode decomposition, Proc. R. Soc. A Math. Phys. Eng. Sci. 466 (2010) 1291–1302. doi:10.1098/rspa.2009.0502.

[13] A. Sadhu, An integrated multivariate empirical mode decomposition method towards modal identification of structures, J. Vib. Control. 23 (2017) 2727–2741. doi:10.1177/1077546315621207.

[14] F. Poncelet, G. Kerschen, J.-C. Golinval, D. Verhelst, Output-only modal analysis using blind source separation techniques, Mech. Syst. Signal Process. 21 (2007) 2335–2358. doi:10.1016/j.ymssp.2006.12.005.

[15] F. Amini, Y. Hedayati, Underdetermined blind modal identification of structures by earthquake and ambient vibration measurements via sparse component analysis, J. Sound Vib. 366 (2016) 117–132. doi:10.1016/j.jsv.2015.10.028.

[16] S. Qin, J. Guo, C. Zhu, Sparse Component Analysis Using Time-Frequency Representations for Operational Modal Analysis, Sensors. 15 (2015) 6497–6519. doi:10.3390/s150306497.

[17] K. Yu, K. Yang, Y. Bai, Estimation of modal parameters using the sparse component analysis based underdetermined blind source separation, Mech. Syst. Signal Process. 45 (2014) 302–316. doi:10.1016/j.ymssp.2013.11.018.

[18] A. Sadhu, S. Narasimhan, A decentralized blind source separation algorithm for ambient modal identification in the presence of narrowband disturbances, Struct. Control Heal. Monit. 21 (2014) 282–302. doi:10.1002/stc.1558.

[19] S.F. Ghahari, F. Abazarsa, M.A. Ghannad, M. Çelebi, E. Taciroglu, Blind modal identification of structures from spatially sparse seismic response signals, Struct. Control Heal. Monit. 19 (2013) n/a-n/a. doi:10.1002/stc.1593.

[20] Y. Yang, S. Nagarajaiah, Output-only modal identification with limited sensors using sparse component analysis, J. Sound Vib. 332 (2013) 4741–4765. doi:10.1016/j.jsv.2013.04.004.

[21] L. De Lathauwer, J. Castaing, Blind Identification of Underdetermined Mixtures by Simultaneous Matrix Diagonalization, IEEE Trans. Signal Process. 56 (2008) 1096–1105. doi:10.1109/TSP.2007.908929.

[22] F. Abazarsa, S.F. Ghahari, F. Nateghi, E. Taciroglu, Response-only modal identification of structures using limited sensors, Struct. Control Heal. Monit. 20 (2013) 987–1006. doi:10.1002/stc.1513.

[23] F. Abazarsa, F. Nateghi, S.F. Ghahari, E. Taciroglu, Extended Blind Modal Identification Technique for Nonstationary Excitations and Its Verification and Validation, J. Eng. Mech. 142 (2016) 4015078. doi:10.1061/(ASCE)EM.1943-7889.0000990.

[24] A. Sadhu, A. Goldack, S. Narasimhan, Ambient modal identification using multi-rank parallel factor decomposition, Struct. Control Heal. Monit. 22 (2015) 595–614. doi:10.1002/stc.1706.

[25] P. Friesen, A. Sadhu, Performance of tensor decomposition-based modal identification under

nonstationary vibration, Smart Mater. Struct. 26 (2017) 35024. doi:10.1088/1361-665X/aa5438.

[26] A. Sadhu, S. Narasimhan, A. Goldack, Decentralized Modal Identification of a Pony Truss Pedestrian Bridge Using Wireless Sensors, J. Bridg. Eng. 19 (2014) 4014013. doi:10.1061/(ASCE)BE.1943-5592.0000552.

[27] B. Hazra, A. Sadhu, A.J. Roffel, S. Narasimhan, Hybrid Time-Frequency Blind Source Separation Towards Ambient System Identification of Structures, Comput. Civ. Infrastruct. Eng. 27 (2012) 314–332. doi:10.1111/j.1467-8667.2011.00732.x.

[28] A. Sadhu, B. Hazra, S. Narasimhan, Decentralized modal identification of structures using parallel factor decomposition and sparse blind source separation, Mech. Syst. Signal Process. 41 (2013) 396–419. doi:10.1016/j.ymssp.2013.06.031.

[29] Y. Yang, S. Nagarajaiah, Blind modal identification of output-only structures in time-domain based on complexity pursuit, Earthq. Eng. Struct. Dyn. 42 (2013) 1885–1905. doi:10.1002/eqe.2302.

[30] A. Sadhu, S. Narasimhan, J. Antoni, A review of output-only structural mode identification literature employing blind source separation methods, Mech. Syst. Signal Process. 94 (2017) 415–431. doi:10.1016/j.ymssp.2017.03.001.

[31] P. Comon, C. Jutten, Sparse component analysis, in: Handb. Blind Source Sep. Indep. Compon. Anal. Appl., Academic Press, 2010.

[32] F. Abrard, Y. Deville, A time-frequency blind signal separation method applicable to underdetermined mixtures of dependent sources, Signal Processing. 85 (2005) 1389–1403. doi:10.1016/j.sigpro.2005.02.010.

[33] V.G. Reju, S.N. Koh, I.Y. Soon, An algorithm for mixing matrix estimation in instantaneous blind source separation, Signal Processing. 89 (2009) 1762–1773. doi:10.1016/j.sigpro.2009.03.017.

[34] S. Gribonval, Rémi;Lesage, A survey of Sparse Component Analysis for Blind Source Separation: principles, perspectives, and new challenges, in: Eur. Symp. Artif. Neural Networks, 2006: pp. 323–330.

[35] Y.P. Raykov, A. Boukouvalas, F. Baig, M.A. Little, What to Do When K-Means Clustering Fails: A Simple yet Principled Alternative Algorithm, PLoS One. 11 (2016) e0162259. doi:10.1371/journal.pone.0162259.

[36] E. van den Berg, M.P. Friedlander, Probing the Pareto Frontier for Basis Pursuit Solutions, SIAM J. Sci. Comput. 31 (2009) 890–912. doi:10.1137/080714488.

[37] E. van den Berg, M.P. Friedlander, {SPGL1}: A solver for large-scale sparse reconstruction, (2007). http://www.cs.ubc.ca/labs/scl/spgl1.

[38] J.M. Caicedo, Practical guidelines for the natural excitation technique (NExT) and the eigensystem realization algorithm (ERA) for modal identification using ambient vibration, Exp. Tech. 35 (2011) 52–58. doi:10.1111/j.1747-1567.2010.00643.x.

[39] J.M.W. Brownjohn, H. Hao, T.-C. Pan, Assessment of structural condition of bridges by dynamic measurements Applied Research Report RG5/97, 2001. http://vibration.ex.ac.uk/doc/10174972.pdf.

[40] D. Hester, J. Brownjohn, M. Bocian, Y. Xu, A. Quattrone, Using inertial measurement units originally developed for biomechanics for modal testing of civil engineering structures, Mech. Syst. Signal Process. 104 (2018) 776–798. doi:10.1016/j.ymssp.2017.11.035.

[41] E. Van Den Berg, M.P. Friedlander, SPGL1: A solver for large-scale sparse reconstruction, (2007). http://www.cs.ubc.ca/labs/scl/spgl1.

[42] E. Van Den Berg, M.P. Friedlander, Probing the Pareto Frontier for Basis Pursuit Solutions, SIAM J. Sci. Comput. 31 (2009) 890–912. doi:10.1137/080714488.

[43] D. Cantero, D. Hester, J. Brownjohn, Evolution of bridge frequencies and modes of vibration during truck passage, Eng. Struct. 152 (2017) 452–464. doi:10.1016/j.engstruct.2017.09.039.

[44] J.M.W. Brownjohn, M. Bocian, D. Hester, A. Quattrone, W. Hudson, D. Moore, S. Goh, M.S. Lim, Footbridge system identification using wireless inertial measurement units for force and response measurements, J. Sound Vib. 384 (2016) 339–355. doi:10.1016/j.jsv.2016.08.008.